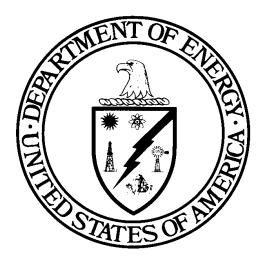# Title 40 CFR Part 191
Subparts B and C
Compliance Recertification
Application
for the
Waste Isolation Pilot Plant

Appendix PORSURF-2009
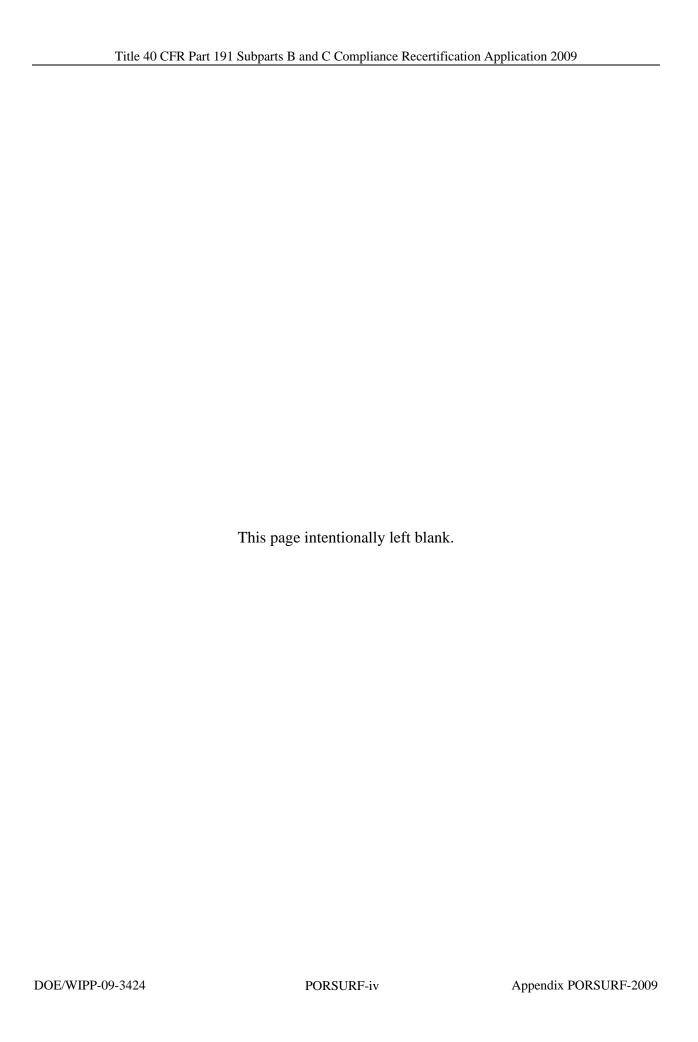## Porosity Surface

United States Department of Energy
Waste Isolation Pilot Plant

Carlsbad Field Office
Carlsbad, New Mexico

Appendix PORSURF-2009
Porosity Surface

Table of Contents

List of Figures

This page intentionally left blank.

Acronyms and Abbreviations

CCA	Compliance Certification Application
CRA	Compliance Recertification Application
K	Kelvin
mol	mole
PA	Performance Assessment
WIPP	Waste Isolation Pilot Plant

This page intentionally left blank.

1 PORSURF-1.0 Introduction

2 Both creep closure of the salt and the presence of either brine or gas in the waste disposal region
3 influence time-dependent changes in void volume in the waste disposal area. As a consequence,
4 these processes influence two-phase fluid flow of brine and gases through the disposal area and
5 its capacity for storing fluids. For performance assessment (PA), a porosity surface method is
6 used to indirectly couple mechanical closure with two-phase fluid flow calculations implemented
7 in the BRAGFLO code (see Appendix PA-2009, Section PA-4.2). The porosity surface
8 approach is used because current codes are not capable of fully coupling creep closure, waste
9 consolidation, brine availability, and gas production and migration. The porosity surface method
10 incorporates the results of closure calculations obtained from the SANTOS code, a quasistatic,
11 large-deformation, finite-element structural analysis code (Stone 1997a). The adequacy of the
12 method is documented in Freeze (1996), who concludes that the approximation is valid so long
13 as the rate of room pressurization in final calculations is bounded by the room pressurization
14 history used to develop the porosity surface.

15 The porosity surface used in the 2009 Compliance Recertification Application (CRA-2009) PA
16 is the same surface used for the Compliance Certification Application (CCA) (U.S. Department
17 of Energy 1996) and the 2004 Compliance Recertification Application (CRA-2004) (U.S.
18 Department of Energy 2004). Consequently, the models and parameters used to calculate this
19 surface are unchanged from the CCA PA. For information on the porosity surface used in the
20 CCA PA, see the CCA, Appendix PORSURF.

21 A separate analysis considered the potential effects on repository performance of uncertainty in
22 the porosity surface (Appendix MASS-2009, Section MASS-21.0). Uncertainty in the porosity
23 surface can arise from heterogeneity in the rigidity of waste packages and from uncertain spatial
24 arrangements of waste in the repository. The analysis considered four porosity surfaces,
25 including the surface from the CCA, which represented various bounding combinations of waste
26 package rigidity and waste initial porosity. The analysis concluded that uncertainty in the
27 porosity surface did not have significant effects on repository performance, and recommended
28 the continued use of the CCA porosity surface in PA.

1 # PORSURF-2.0 Creep Closure Method

2 Creep closure is accounted for in BRAGFLO by changing the porosity of the waste disposal area
3 according to a table of porosity values, termed the porosity surface. The porosity surface is
4 generated using SANTOS, a nonlinear finite element code. Disposal room porosity is calculated
5 over time, for different rates of gas generation and gas production potential, to construct a three-
6 dimensional porosity surface representing changes in porosity as a function of pressure and time
7 over the 10,000-year simulation period.

8 The completed porosity surface is compiled in tabular form and is used in the solution of the gas
9 and brine mass balance equations presented in Appendix PA-2009, Section PA-4.2.1. Porosity is
10 interpolated from the porosity surface corresponding to the calculated gas pressure at time step
11 t_n. This is done iteratively, as decreases in the porosity will increase the pressure. The closure
12 data provided by SANTOS can be viewed as a series of surfaces, with any gas generation history
13 computed by BRAGFLO constrained to fall on this surface. Various techniques described in
14 Freeze, Larson, and Davies (1995) were used to check the validity of this approach, and it was
15 found to be a reasonable representation of the behavior observed in the complex models.

16 In SANTOS, the gas pressure in the disposal room at time t_n is computed from the ideal gas law
17 by the following relationship:

18
$$p_g = \frac{NRT}{V}$$

19 where N is the number of moles of gas at time t_n, R is the universal gas constant (8.31
20 m^3·Pa/mol·K), T is the absolute temperature in degrees Kelvin (constant at 300 K), and V is the
21 free volume of the room at time t_n. The number of moles of gas is computed as

22
$$N_t = N_{t-1} + N_{drums} \times f \times r(t) \times (t_n - t_{n-1})$$

23 where $r(t)$ is the gas generation rate (mol/drum/yr) at time t for the scaling factor f and N_{drums} is
24 the number of drums of waste in the room (6804 drums/room). The base gas generation rate in
25 SANTOS is

26
$$r(t) = \begin{cases} 2 \ mol \, / \, drum \, / \, yr, & 0 \le t \le 550 \ yr \\ 1 \ mol \, / \, drum \, / \, yr, & 550 \ yr < t \le 1050 \ yr \\ 0 \ mol \, / \, drum \, / \, yr, & 1050 \ yr < t \end{cases}$$

27 The base gas generation rate $r(t)$ is representative of relatively high gas production rates from
28 both microbial degradation of cellulosic, plastic, and rubber materials and from anoxic corrosion
29 of Fe-base metals (Appendix PA-2009, Section PA-4.2.5; Butcher 1997a). To provide a range of
30 SANTOS results that spans the possible range of pressure computed by BRAGFLO, the gas
31 generation rate is varied by the scaling factor f. Thirteen values of f are used to construct the
32 porosity surface: f = 0.0, 0.025, 0.05, 0.1, 0.2, 0.4, 0.5, 0.6, 0.8, 1.0, 1.2, 1.6, and 2.0. The
33 condition f = 0 represents the state of the repository when no gas is produced; f = 2 represents
34 twice the base gas generation rate.

1   In SANTOS, gas generation is included to introduce a range of values for gas pressure during
2   room closure, thereby capturing the effects of gas pressure on room closure; the use of the
3   scaling factor f ensures that SANTOS results span a wide range of possible gas generation rates
4   and potentials.

PORSURF-3.0 Conceptual Model for Porosity Surface

The ability of salt to deform with time, eliminate voids, and create an impermeable barrier around the waste was one of the principal reasons for locating the Waste Isolation Pilot Plant (WIPP) repository in a bedded salt formation (National Academy of Sciences-National Research Council 1957, pp. 4–5). The creep closure process is a complex and interdependent series of events starting after a region within the repository is excavated. Immediately upon excavation, the equilibrium state of the rock surrounding the repository is disturbed, and the rock begins to deform and return to equilibrium. Eventually, at equilibrium, deformation ceases, as the waste region has undergone as much compaction as is possible under the prevailing lithostatic stress field and the differential stresses in the salt approach zero.

Creep closure of a room begins immediately upon excavation and causes the volume of the cavity to decrease. If the room were empty, rather than partially filled with waste, closure would proceed until the void volume created by the excavation is eliminated; the surrounding halite would then return to its undisturbed, uniform stress state. In a waste-filled room, the rock will contact the waste and the rate of closure will decrease as the waste compacts and stiffens; eventually, closure will cease when the waste can take the full overburden load without further deformation. Initially, unconsolidated waste can support only small loads, but as the room continues to close after contact with the waste, the waste will consolidate and support a greater portion of the overburden load.

The presence of gas in the room will retard the closure process due to pressure buildup. As the waste consolidates, pore volume is reduced and pore pressure increases (using the ideal gas law). In this process, the waste can be considered to be a skeleton structure immersed in a pore fluid (the gas). As the pore pressure increases, less overburden weight is carried by the skeleton, and more support is provided by the gas. If the gas pressure increases to lithostatic pressure, the pore pressure alone is sufficient to support the overburden.

1 PORSURF-4.0 SANTOS Numerical Analyses

2 Computing repository creep closure is a particularly challenging structural engineering problem
3 because the rock surrounding the repository continually deforms with time until equilibrium is
4 reached. Not only is the deformation of the salt inelastic, but it also involves larger deformations
5 that are not customarily addressed with conventional structural deformation codes. In addition,
6 the formation surrounding the repository is inhomogeneous in composition, containing various
7 parting planes and interbeds with different properties than the salt.

8 Waste deformation is also nonlinear, with large strains, and the response of a waste-filled room
9 is complicated by the presence of gas. These complex characteristics of the materials making up
10 the repository and its surroundings require the use of highly specialized constitutive models.
11 Appropriate models have been built into the SANTOS code over a number of years. Principal
12 components of these models include the following:

13 1. Disposal Room Configuration and Idealized Stratigraphy. Disposal room dimensions,
14   computational configuration, and idealized stratigraphy are defined in the CCA, Appendix
15   PORSURF, Attachment 1. The idealized stratigraphy is reproduced in Figure PORSURF-1.

16 2. Discretized Finite Element Model. A two-dimensional plane strain model, shown in Figure
17   PORSURF-2, is used for the SANTOS analyses. The discretized model represents the room
18   as one of an infinite number of rooms located at the repository horizon. The model contains
19   1,680 quadrilateral uniform-strain elements and 1,805 nodal points. Contact surfaces
20   between the emplaced waste and the surfaces of the room are addressed. The justification for
21   this model and additional detail on initial and boundary conditions are provided in the CCA,
22   Appendix PORSURF, Attachment 1.

23 3. Geomechanical Model. Mechanical material response models and their corresponding
24   property values are assigned to each region of the configuration. These models include:

25 A. A combined transient-secondary creep constitutive model for clean and argillaceous
26   halite

27 B. An inelastic constitutive model for anhydrite

28 C. A volumetric plasticity model for the emplaced waste

29 Material properties are provided in the CCA, Appendix PORSURF, Attachment 1.

30 The results of the SANTOS calculations are illustrated in Figure PORSURF-3 and Figure
31 PORSURF-4. Figure PORSURF-3 shows disposal room porosity as a function of time for
32 various values of the gas generation scaling factor f. Figure PORSURF-4 shows disposal room
33 pressure as a function of time for various values of f. When $f = 0$, no gas is present in the
34 disposal room; thus, disposal room pressure is identically zero for all times. This pressure curve
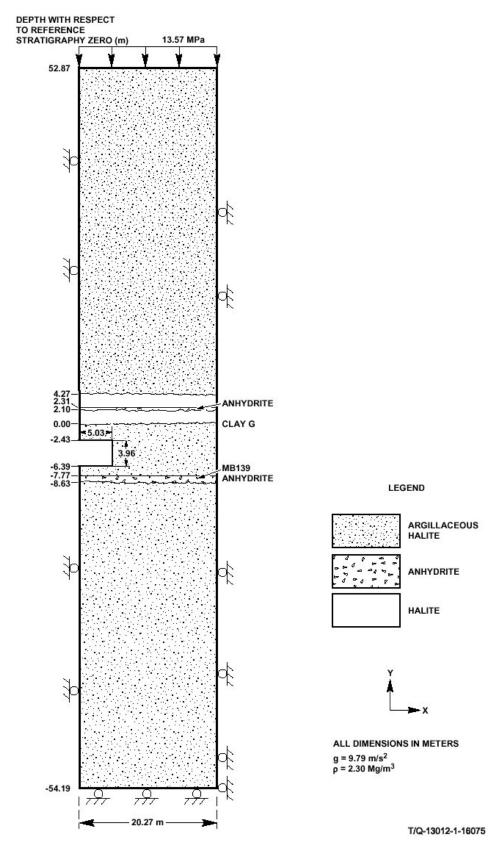35 is omitted from Figure PORSURF-4.

1

2 **Figure PORSURF-1. Stratigraphy Used for the Porosity Surface Calculations**

**Applied Traction
13.57 MPa**

52.87 m

$g=9.79$ m/s^2

$U_x=0.0$ $U_x=0.0$

5.03 m

adaptive internal
pressure, p_g

2.676 m

3.96 m

20.27 m

3.675 m

-54.19 m

Y

X

$U_y=0.0$

	Halite		Anhydrite
	Argillaceous Halite		Waste

1

2   **Figure PORSURF-2.   Mesh Discretization and Boundary Conditions Used for the Porosity**
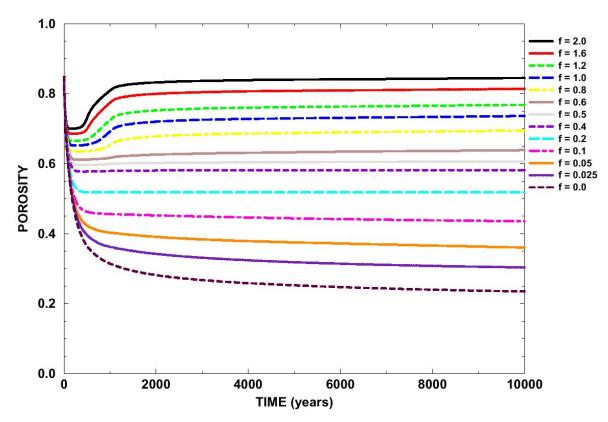3   **Surface Calculations**

1

2 **Figure PORSURF-3. Disposal Room Porosity for Various Values of the Scaling Factor *f***
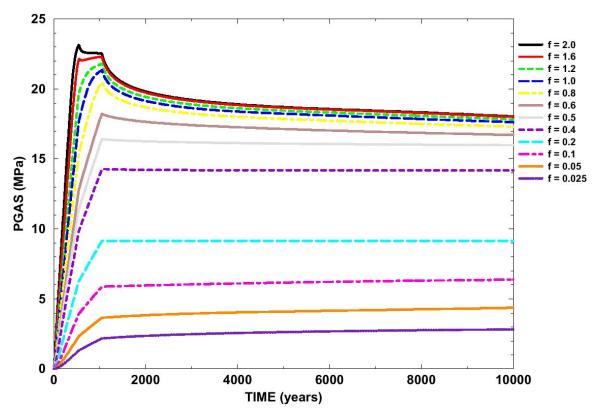

3

4 **Figure PORSURF-4. Disposal Room Pressure for Various Values of the Scaling Factor *f***

1 # PORSURF-5.0 Implementation of Porosity Surface in BRAGFLO

2 As outlined above, the SANTOS program is used to calculate time-dependent porosities and
3 pressures in the repository for a range of gas generation rates determined by the scaling factor f.
4 Calculation with each value of f results in the porosity and pressure curves in Figure PORSURF-
5 3 and Figure PORSURF-4.

6 The porosity calculated by SANTOS is the intrinsic, or true, porosity, which is defined as the
7 ratio of the void volume to the current volume of a (deformable) element of waste. In contrast,
8 porosity in BRAGFLO is defined as the ratio of void volume to the original volume of an
9 element of waste. Mathematically, the BRAGFLO porosity, ϕ_B, and the intrinsic porosity in
10 SANTOS, ϕ, are defined as

11
$$\phi_B = \frac{V_{void}}{V_0}$$
$$\phi = \frac{V_{void}}{V}$$

12 where V_{void} is the current void volume, V_0 is the original (total) volume, and V is the current
13 (total) volume of a waste element.

14 The porosities shown in Figure PORSURF-3 are the porosities calculated by SANTOS to be
15 used in BRAGFLO. The BRAGFLO porosities are related to the porosities calculated by
16 SANTOS by correcting for deformation of the waste during repository closure. The relationship
17 between ϕ_B and ϕ is given by

18
$$\phi_B = \frac{1 - \phi_0}{1 - \phi} \phi$$

19 where ϕ_0 is the initial porosity of the waste. Note that the values of ϕ_B and ϕ are equal at the
20 initial porosity before the waste starts to compact.

21 Brine pressures $p_b(t)$ obtained in the waste disposal regions are used in conjunction with the
22 results in Figure PORSURF-3 and Figure PORSURF-4 to estimate porosity in the waste-filled
23 regions for the BRAGFLO calculations. In the CRA-2009 PA, brine pressure and gas pressure
24 are set as equal in the waste-filled regions, i.e. capillary pressure is not included (see Appendix
25 PA-2009, Section PA-4.2). This is unchanged from the CCA and CRA-2004 PAs.

26 Given a value for $p(t)$, BRAGFLO looks at the porosity surface to find indices for times in the
27 porosity table so that

28
$$t_1 \leq t \leq t_2$$

29 Next, BRAGFLO determines whether the current pressure is above the pressure curve in the
30 interpolation table corresponding to the maximum f value or corresponding to the minimum f

1   value in the table. If p lies above the curve formed by the points $(t_1, p(t_1, f_{max}))$ and

2      $(t_2, p(t_2, f_{max}))$, the porosity is calculated by interpolation using the following formula:

3
$$\phi = \phi(t_1, f_{max}) + \frac{\phi(t_2, f_{max}) - \phi(t_1, f_{max})}{t_2 - t_1}(t - t_1)$$

4   Similarly, if p lies below the curve formed by the points $(t_1, p(t_{1,} f_{min}))$ and $(t_2, p(t_2, f_{min}))$, the

5   porosity is calculated by interpolation using the following formula:

6
$$\phi = \phi(t_1, f_{min}) + \frac{\phi(t_2, f_{min}) - \phi(t_1, f_{min})}{t_2 - t_1}(t - t_1)$$

7   For values of p that do not lie above or below the maximum and minimum $p(t, f)$ curves in the
8   interpolation table, BRAGFLO finds f values f_1 and f_2 so that the point (t, p) lies between two
9   curves $(t, p(t, f_1))$ and $(t, p(t, f_2))$. This is illustrated in Figure PORSURF-5.
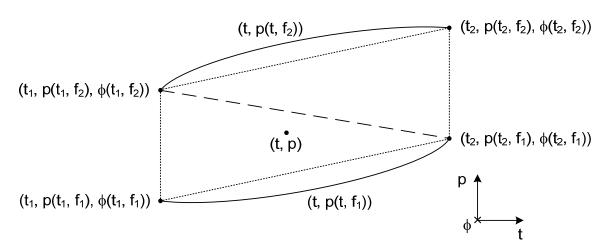

10

11   **Figure PORSURF-5. Location of Points in Porosity Table around Point (t, p)**

12   Interpolation is performed on the triangle formed by the set of points that encloses the point $(t,$
13      $p)$. For example, in Figure PORSURF-5, the points constituting the lower triangle would be used
14   for interpolation. Interpolation on the triangle is calculated from the areas of the three triangles
15   in the plane of t and p that can be formed from the point (t, p) and the vertices of the enclosing
16   triangle, as illustrated in Figure PORSURF-6. The porosity is then calculated from

17
$$\phi(t, p) = \frac{A_1}{A}\phi(t_1, f_2) + \frac{A_2}{A}\phi(t_1, f_1) + \frac{A_3}{A}\phi(t_2, f_1)$$

18   where A is the total area of the triangles $(A_1 + A_2 + A_3)$ in Figure PORSURF-6.

19   At $t = 0$ (i.e., immediately after the operational period; see Appendix PA-2009, Section PA-4.2),
20   interpolation is performed using the points $(t_1, p(t_1, f_1), \phi(t_1, f_1))$, $(t_2, p(t_2, f_1), \phi(t_2, f_1))$, and
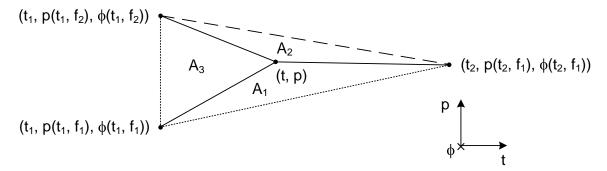
21

Figure PORSURF-6 contains:
- $(t_1, p(t_1, f_2), \phi(t_1, f_2))$
- A_2
- A_3
- (t, p)
- A_1
- $(t_2, p(t_2, f_1), \phi(t_2, f_1))$
- $(t_1, p(t_1, f_1), \phi(t_1, f_1))$
- p
- ϕ
- t

1

2   **Figure PORSURF-6. Triangular Interpolation to Determine the Porosity at (t, p)**

3      $(t_2, p(t_2, f_2), \phi(t_2, f_2))$. This is because at $t = 0$, the two points vertically separated in Figure

4   PORSURF-6 at t_1 are equal (the porosity is equal to the initial value at $t = 0$ for all values of f).

PORSURF-6.0 Dynamic Closure of the North End and Hallways

The porosity surface method is not used to model the north end of the repository occupied by the experimental and operational regions. During development of the CCA PA, a supporting analysis compared brine and gas flow results for two models for closure of the north end of the repository: a dynamic closure model and a baseline model, in which the porosity and permeability of these regions were held constant (Vaughn, Lord, and MacKinnon 1995). The study examined the effect of these two approaches on brine releases to the accessible environment for both disturbed and undisturbed conditions, as well as the effects on brine pressures and brine saturations in the modeled regions. The study concluded that the baseline case (assuming constant low porosity and high permeability) consistently led to either similar or more conservative brine pressures and brine saturations, thereby overestimating potential releases relative to the dynamic consolidation case. Consequently, PA uses the simplifying case of constant porosity and permeability in the north end of the repository, rather than modeling dynamic closure of these areas.

1 PORSURF-7.0 Additional Information

2 The following attachments were included in the CCA, Appendix PORSURF to document
3 additional details of the porosity surface method:

4 1. The CCA, Appendix PORSURF, Attachment 1, *Proposed Model for the Final Porosity*
5 *Surface Calculations*. This memo documents preliminary configuration and constitutive
6 property values for the final porosity surface calculations. Tables in the memo include
7 elastic and creep properties for clean halite and argillaceous halite, volumetric strain data and
8 material constants used in the volumetric-plasticity model for waste, and elastic and Drucker-
9 Prager constants assigned to anhydrite Marker Bed 139. This attachment was supplemented
10 and updated subsequent to the CCA by Butcher (1997a and 1997b).

11 2. The CCA, Appendix PORSURF, Attachment 2, *Baseline Inventory Assumptions for the*
12 *Final Porosity Surface Calculations*. This memo discusses the effect of changes in the
13 Transuranic Waste Baseline Inventory Report on the SANTOS analyses.

14 3. The CCA, Appendix PORSURF, Attachment 3, *Corrosion and Microbial Gas Generation*
15 *Potentials*. This memo discusses the rationale for the base gas production potentials of 1,050
16 mol per drum for corrosion and 550 mol per drum for microbial decay in the SANTOS
17 analyses.

18 4. The CCA, Appendix PORSURF, Attachment 4, *Resolution of Remaining Issues for the Final*
19 *Disposal Room Calculations*. This memo provides additional detail on the disposal room
20 elevation, determination of plastic constants for transuranic waste, and determination of
21 SANTOS input constants for clean halite, argillaceous halite, and anhydrite.

22 5. The CCA, Appendix PORSURF, Attachment 5, *Sample SANTOS Input File for Disposal*
23 *Room Analysis*. A representative sample input file is provided in this attachment. The only
24 difference between this input file and the file used in the CCA calculations (see Stone 1997b)
25 is a subroutine modifying the gas generation variable.

26 6. The CCA, Appendix PORSURF, Attachment 6, *Final Porosity Surface Data*. This
27 attachment provides SANTOS results for selected gas generation scaling factors $f = 0.5, 1.0,$
28 and 2.0. This attachment was updated and published as a formal SAND report (Stone 1997b)
29 subsequent to submittal of the CCA.

30 7. The CCA, Appendix PORSURF, Attachment 7, *SANTOS – A Two-Dimensional Finite*
31 *Element Program for the Quasistatic, Large Deformation, Inelastic Response of Solids*. This
32 report documents the SANTOS code.

PORSURF-8.0 References

Butcher, B.M. 1997a. *A Summary of the Sources of Input Parameter Values for the Waste Isolation Pilot Plant Final Porosity Surface Calculations*. SAND97-0796. Albuquerque: Sandia National Laboratories.

Butcher, B.M. 1997b. *Waste Isolation Pilot Plant Disposal Room Model*. SAND97-0794. Albuquerque: Sandia National Laboratories.

Freeze, G.A. 1996. *Repository Closure–Reasoned Argument for FEP Issue DR12*. ERMS 413328. Albuquerque: Sandia National Laboratories.

Freeze, G.A., K.W. Larson, and P.B. Davies. 1995. *Coupled Multiphase Flow and Closure Analysis of Repository Response to Waste-Generated Gas at the Waste Isolation Pilot Plant (WIPP)*. SAND93-1986. Albuquerque: Sandia National Laboratories.

National Academy of Sciences-National Research Council (NAS-NRC). 1957. *The Disposal of Radioactive Waste on Land.* Publication 519. Washington, DC: National Academy of Sciences.

Stone, C.M. 1997a. *SANTOS—A Two-Dimensional Finite-Element Program for the Quasistatic, Large Deformation, Inelastic Response of Solids*. SAND90-0543. Albuquerque: Sandia National Laboratories.

Stone, C.M. 1997b. *Final Disposal Room Structural Response Calculations*. SAND97-0795. Albuquerque: Sandia National Laboratories.

U.S. Department of Energy (DOE). 1996. *Title 40 CFR Part 191 Compliance Certification Application for the Waste Isolation Pilot Plant* (October). 21 vols. DOE/CAO 1996-2184. Carlsbad, NM: Carlsbad Area Office.

U.S. Department of Energy (DOE). 2004. *Title 40 CFR Part 191 Compliance Recertification Application for the Waste Isolation Pilot Plant* (March). 10 vols. DOE/WIPP 2004-3231. Carlsbad, NM: Carlsbad Field Office.

Vaughn, P., M. Lord, and B. MacKinnon. 1995. Memorandum to D.R. Anderson (Subject: FEP Screening Issue DR-3). 21 December 1995. ERMS 230794. U.S. Department of Energy, Sandia National Laboratories, Albuquerque, NM.